Journal of Molecular Catalysis A: Chemical 287 (2008) 176–181

Contents lists available at ScienceDirect

Journal of Molecular Catalysis A: Chemical

journal homepage: www.elsevier.com/locate/molcata

The characterization of ZnO–anatase–rutile three-component semiconductor and enhanced photocatalytic activity of nitrogen oxides

Haiqiang Wang, Zhongbiao Wu*, Yue Liu, Zhongyi Sheng

Department of Environmental Engineering, Zhejiang University, Zhe Da Road, No. 38, Hangzhou 310027, Zhejiang, PR China

ARTICLE INFO

Article history:
Received 13 June 2007
Received in revised form 19 January 2008
Accepted 9 March 2008
Available online 15 March 2008

Keywords:
NO
Photocatalyst
ZnO–anatase–rutile
Zinc ion
Three-component semiconductor

ABSTRACT

Three-component semiconductors just like ZnO–anatase–rutile with different zinc ion content (between 0.1 and 10.0 at%) were prepared by a wet impregnation method and investigated with respect to their behavior in UV photocatalytic oxidation of nitric oxide. The results were correlated with structural, electronic and surface examinations of the catalysts by using X-ray diffraction (XRD) analysis, X-ray photoelectron spectrum (XPS) analysis, transmission electron microscopy (TEM), ultraviolet–visible absorbance spectra (UV–vis) and photoluminescence (PL) spectra. Firstly, it was found that the OH^- species were improved on the surface of ZnO–anatase–rutile three-component system, which was favorable for the oxidation of NO by interrupting the formation of adsorbed nitrolysis. Secondly, the lifetime of electrons and holes was prolonged in the ZnO–anatase–rutile three-component system and the enhancement of the photocatalytic activity was observed for the Zn^{2+} doping concentration ranged from 0.1 to 2.0 at%.

1. Introduction

The worsening of one's living environment due to NOx has constituted a serious social problem. Nitrogen oxides (NOx) exhausted from furnaces have caused various environmental problems such as acid rain, photochemical smog and greenhouse effect [1–2]. To reduce the emissions of NOx into atmosphere, various processes, including combustion modifications, dry processes and wet processes have been developed [3–5].

Wet processes are very efficient to remove NO_2 from flue gas. However, NO is difficult to be removed by wet processes because of its low solubility in aqueous solution [6–7]. The photocatalytic oxidation (PCO) may be an economical and environmental-friendly approach to transform the NO to NO_2 and finally improve the absorption efficiency of wet processes [8–9]. Unfortunately, most of the previous investigations about the PCO of NOx were focused on the removal of NO from ambient environment (either indoor or outdoor air) [10–16]. Compared with NOx from flue gas, the concentration of NO from ambient environment is much lower. For the treatment of NO from flue gas, it is necessary to develop more effective ways to enhance the photocatalytic efficiency of NO.

Doping metal ions and coupling semiconductors are often adopted as effective modification methods to improve the performance of TiO_2. A wide range of metal ions (Fe, Zn, V, Cr, Mn, Cu, Co, Mo, etc.) in combination with the use of TiO_2 particles have been investigated [17–19]. But for the photocatalytic oxidation of NO, NO adsorb on the M/TiO_2 in the form of nitrosyls which will decrease the oxidation rate of NO (M = Cu, V, Cr, Fe, Mo, Mn) [19–21]. Nowadays, doping Zn ions or coupling ZnO with TiO_2 has received a lot of attention because of the special electronic properties of ZnO [22–26]. For the oxidation of NO, the hydroxyl existing on the surface of ZnO can prevent the formation of nitrosyls just like TiO_2 (anatase or rutile). Also, the band gap energy of ZnO is approximately 3.2 eV and the intrinsic semiconducting characteristics of ZnO and TiO_2 are different. Thus, constructing a three-component ZnO–anatase–rutile semiconductor will be a promising way to enhance the photocatalytic efficiency of NO.

In this article, the photocatalytic activity of the three-component ZnO–anatase–rutile semiconductor for the oxidation of NOx was investigated; its characterization was carried out and analyzed in reaction mechanism. The ZnO–anatase–rutile semiconductor was prepared by impregnating ZnO nano-particle on Degussa P25 surface. And the catalysts were characterized by X-ray diffraction (XRD) analysis, ultraviolet–visible (UV–vis) absorption spectroscopy, transmission electron microscopy (TEM), X-ray photoelectron spectrum (XPS) analysis and photoluminescence (PL) spectra.

* Corresponding author. Tel.: +86 571 87952459; fax: +86 571 87953088.
E-mail address: zbwu@zju.edu.cn (Z. Wu).

1381-1169/$ – see front matter © 2008 Elsevier B.V. All rights reserved.
doi:10.1016/j.molcata.2008.03.010

2. Experimental

2.1. Preparation of TiO_2 catalysts

The Degussa P25 TiO_2 powder (anatase:rutile = 8:2, crystal size: 30–50 nm, surface area: $50 \pm 5\ m^2\ g^{-1}$, Degussa Co. Ltd., Germany) was used as bare TiO_2. Samples containing 0.1, 0.5, 1.0, 2.0, 5.0 and 10.0 mole of metal ions over 100 mole of titanium ions were prepared by the wet impregnation method. $Zn(NO_3)_2{\cdot}6H_2O$ as analytical grade was used, and 4 g TiO_2 powder was impregnated with aqueous solutions containing the required amounts of the zinc ions. After aging at room temperature for 1 h, the pH value of the suspension was adjusted to 10.0 by the addition of NH_3 solution ($1.0\ mole\ L^{-1}$), while the suspension was stirred by a magnetic stirrer.

Immobilization was carried out by the dip-coating method. The TiO_2 suspension was gradually dropped and the catalyst was coated on the woven glass fabric (pretreatment: 500 °C for 1 h) over an area of 4 cm × 80 cm. The coated woven glass fabric was treated with a desiccation process in a convection oven at 80 °C for 12 h. Finally, the woven glass fabric was calcined at 400 °C for 1 h. The amount of coated TiO_2 was determined by the mass increase of the woven glass fabric after the coating. In all experiments, the weight of TiO_2 coated was kept as $0.5\ g \pm 10\%$.

2.2. Characterization of TiO_2 catalysts

X-ray diffraction analysis (XRD) of the catalysts was performed on a Rigaku diffractometer (D/Max RA) at 40 kV and 150 mA, at an angle of 2θ from 20° to 80°. The mean crystallite sizes corresponding to anatase (1 0 1) and rutile (1 1 0) were determined by the Scherer equation. The morphology, structure and grain size of TiO_2 particle were examined by TEM and high resolution-transmission electron microscopy (HR-TEM) using a JEM-2010 instrument. Ultraviolet–visible absorbance spectra were recorded with a Purkinje TV-1901 instrument, using $BaSO_4$ as reference sample. XPS analysis was carried out by a V.G. Scientific Escalab 250 instrument with Cu Kα X-rays. PL spectra of the prepared samples were recorded at room temperature with a steady state/lifetime spectrofluorometer (Fluorolog-3-Tau, Jobin Yvon) equipped with a xenon UV–vis-near-IR excitation lamp at an excitation wavelength of 300 nm.

2.3. Photocatalytic reaction

A set of experiments for the removal of NO from a gaseous phase was carried out in the continuous-flow reactor using the catalysts prepared under different conditions. Fig. 1 showed the diagram of the photocatalytic oxidation experimental setup. The experimental setup consisted of the gas supply, PCO reactor and analytical system. The air, NO and N_2 gas streams were mixed to obtain the desired concentration (NOx: 90 ppm; NO: 80 ppm; relative humidity: 80%). The flow rate of the gas was $2.0\ L\ min^{-1}$ and the space time was 10 s. After a stabilized period of about 1 h, outlet NO concentration became the same as that of inlet gas and then the experiment started by turning on the UV lamp.

NO, NO_2 and O_2 were measured with a Kane International Limited Model KM-9106 flue gas analyzer. The relative humidity was measured with a relative humidity analyzer (Testo Co. Ltd., Model 605-H1). The NO conversion was evaluated according to the definition of NO conversion = $(([NO]_{inlet} - [NO]_{outlet})/[NO]_{inlet}) \times 100$.

3. Result and discussion

3.1. Crystal structure and size of ZnO–anatase–rutile catalysts

The XRD spectra of the ZnO–anatase–rutile catalysts with different zinc ion doping concentration were presented in Fig. 2. The anatase (1 0 1) crystal sizes of these catalysts, determined by the Scherer equation, were between 20 and 25 nm, and the rutile (1 1 0) crystal sizes ranged from 50 to 60 nm. The titania crystal size of ZnO-doped catalysts had little change compared with the pure Degussa P25 particles.

From the XRD (Fig. 2), it could be seen that with different doping concentration (0.1–10 at%), none of the XRD spectra showed intense peaks for zinc oxides except the sample f (zinc ions doping concentration 10 at%). It indicated that the low concentration deposition of zinc ions on the TiO_2 surface did not induce the formation of agglomerate ZnO crystal phases. However, the remarkable diffraction peaks (2θ = 31.77°, 34.42°, 36.25°) corresponded to ZnO were observed from curve f, which implied that ZnO had been agglomerated on the TiO_2 surface with a high zinc ions concentration of 10 at%.

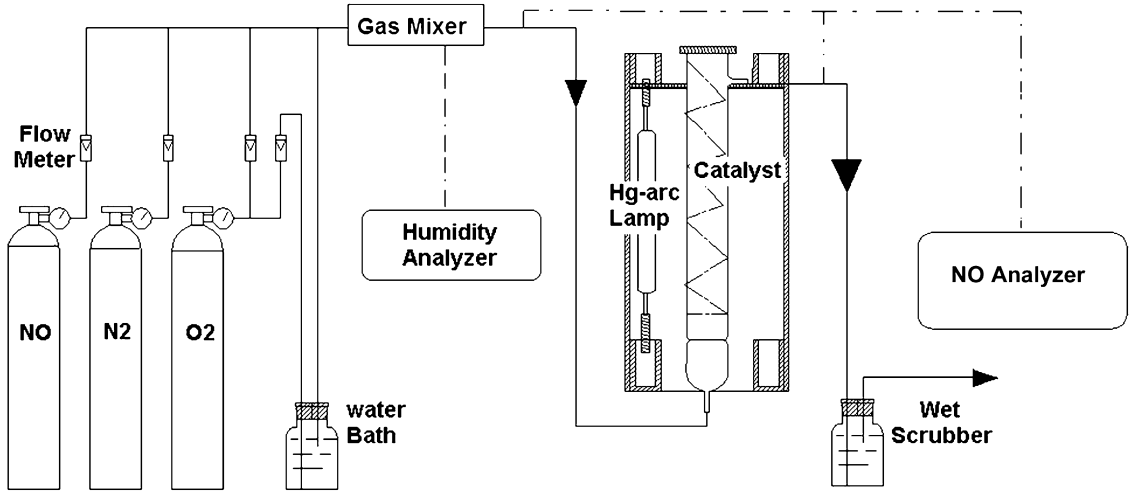

Fig. 1. Diagram of the photocatalytic oxidation experimental setup.

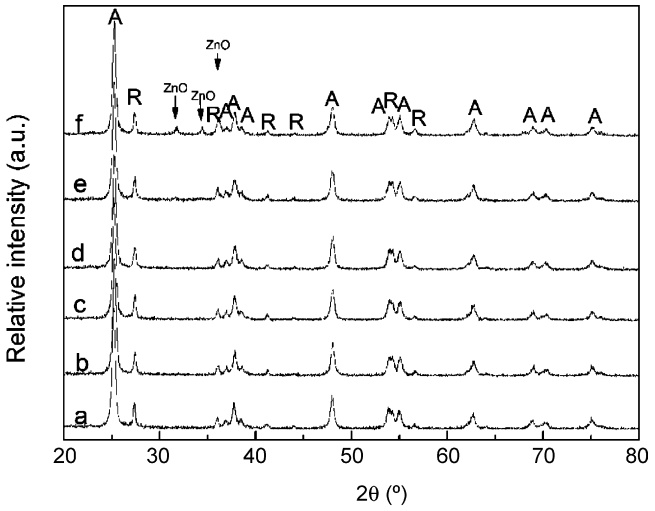

Fig. 2. XRD patterns of Zn^{2+}-doped TiO_2 catalysts with different doping concentration. (a) 0.1 at% Zn^{2+}; (b) 0.5 at% Zn^{2+}; (c) 1.0 at% Zn^{2+}; (d) 2.0 at% Zn^{2+}; (e) 5.0 at% Zn^{2+}; (f) 10.0 at% Zn^{2+}.

3.2. Microstructure and crystallization analysis by TEM and HR-TEM

TEM and HR-TEM micrographs of ZnO-doped TiO_2 particles were shown in Fig. 3. From the TEM micrograph of 0.5 at% ZnO–TiO_2, shown in Fig. 3a, it could be seen that the primary TiO_2 particle sizes ranged from 20 to 50 nm, which were in good agreement with the value of the crystallite size determined by XRD spectra. Furthermore, it could be found that spherical particles (showed by the arrowhead) which corresponded to the zinc oxide were randomly dispersed into the titania particles. It was confirmed that ZnO was well dispersed in the TiO_2 particles. Fig. 3b showed the HR-TEM image of 0.5 at% ZnO–TiO_2. From Fig. 3b, the ZnO particle which deposited on the TiO_2 surface was clearly observed (showed by the arrowhead). Fig. 3c and d were the TEM micrograph and HR-TEM micrograph of 10.0 at% ZnO–TiO_2, respectively. A large amount of spherical particles attributed to ZnO (showed by the arrowhead) were observed in the micrograph. It was confirmed that more ZnO particles were formed on TiO_2 surface under the high doping concentration.

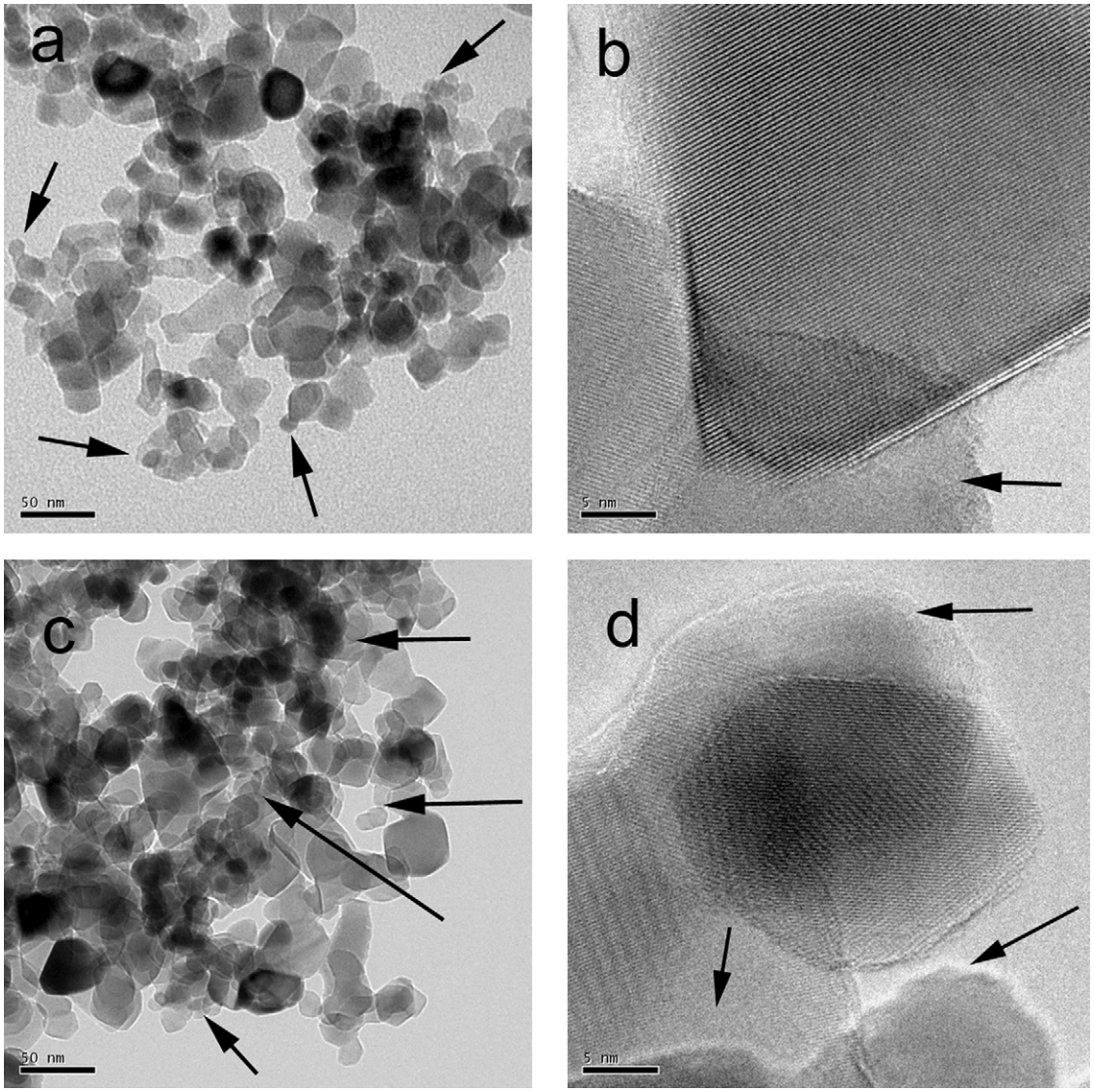

Fig. 3. TEM and HR-TEM micrographs of Zn^{2+}-doped TiO_2 particles. (a) TEM of 0.5 at% Zn^{2+}-doped TiO_2 particles; (b) HR-TEM of 0.5 at% Zn^{2+}-doped TiO_2 particles; (c) TEM of 10.0 at% Zn^{2+}-doped TiO_2 particles; (d) HR-TEM of 10.0 at% Zn^{2+}-doped TiO_2 particles.

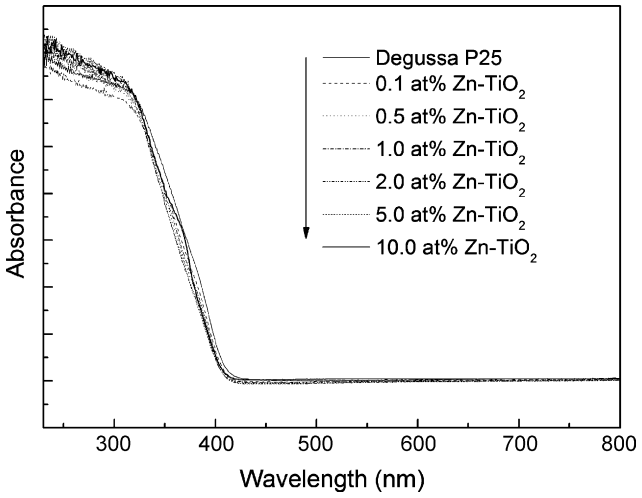

Fig. 4. UV–vis absorbance spectra for the ion-doped titania powder.

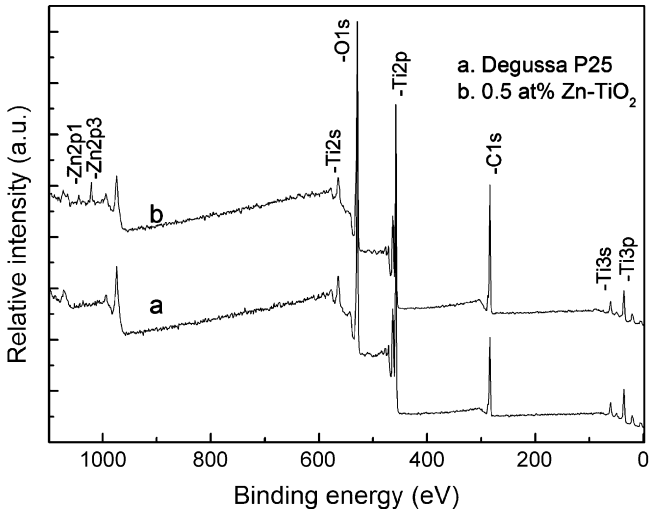

Fig. 5. XPS survey spectrum of 0.5 at% Zn^{2+}-doped TiO_2 particles and Degussa P25.

3.3. UV–vis analysis

UV–vis spectroscopy has been commonly used to investigate the band structure of TiO_2. The absorption spectra of TiO_2 powders with different zinc ions doping concentration were shown in Fig. 4. Inspection of the UV–vis spectra for the different products (Fig. 4), clearly indicated that the absorption edges of ZnO-doped TiO_2 particles had little change compared to that of Degussa P25 TiO_2. It was reported that the band gap energy of ZnO was near to that of TiO_2 (approximately 3.2 eV) [22–23]. Thus, the band gap energies of ZnO-doped TiO_2 particles did not have much change after the ZnO deposition on the TiO_2 surface.

3.4. XPS spectrum of ZnO-doped TiO_2

The XPS results of 0.5 at% ZnO-doped TiO_2 particles and Degussa P25 were shown in Fig. 5. The content and binding energy of all elements in the surface of 0.5 at% ZnO-doped TiO_2 particles and Degussa P25 were shown in Table 1. Among them, the element of C came from the pollution of the instrument. According to XPS measurements with 0.5 at% ZnO-doped TiO_2 particles, a binding energy of Zn $2p_{3/2}$ was determined to be 1021.71 eV, which indicated that Zn existed as Zn^{2+} bonding with oxygen atoms. The binding energies for Ti $2p_{3/2}$ and Ti $2p_{1/2}$ were 485.65 and 464.4 eV, respectively. Based on the peak area ratio, there was about 1.25 at% Zn of TiO_2 in the final product, which was much higher than the designed doping concentration. It could be concluded that ZnO particles were mainly located on the TiO_2 surface.

The high resolution XPS spectra of O 1s in the surface of Degussa P25 and 0.5 at% ZnO-doped TiO_2 were shown in Fig. 6. The peak of O 1s was divided into three peaks, corresponding to Ti–O of TiO_2, hydroxyl group in the surface of the catalyst and C—O bonds [27–28], respectively. Table 2 listed the results of curve fitting of high resolution XPS spectra for the O 1s region of Degussa P25 and

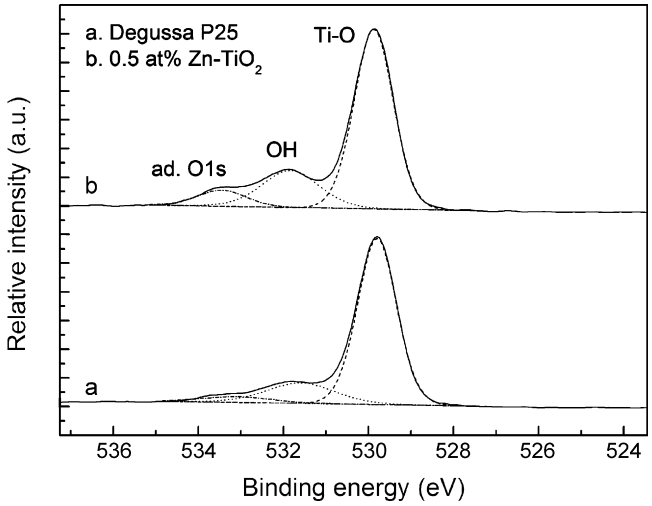

Fig. 6. High resolution XPS spectra of the O 1s region for the different catalysts.

0.25 at% Zn^{2+}-doped TiO_2, where r_i (%) indicated the atomic ratio of each contribution to the total of all the three kinds of oxygen contributions. The C—O bonds in the films were attributed to the organic residues such as alcohol, unhydrolyzed alkoxide groups and CO_3^{2-} [29]. Usually, the physical adsorption of H_2O existing in the surface of the catalyst was easy to be desorbed in the super high vacuum of XPS system. So the hydroxyl groups measured by XPS could not ascribe to the chemisorbed H_2O. As seen in Fig. 2 and Table 2, the hydroxyl group content in 0.5 at% ZnO-doped TiO_2 was higher than that in Degussa P25. In the photocatalytic reactions, a catalyst surface with abundant hydroxyl group was a better producer of hydroxyl radical [30]. Also for the photocatalytic oxidation of NO, the increased hydroxyl content on the surface of photocatalyst would prevent the formation of adsorbed nitrosyls.

Table 1
Composition (at%) and binding energy of the catalysts

Catalysts		Ti2p	O1s	O1s	O1s	C1s	C1s	C1s	Zn2p
Degussa P25	at%	16.38	2.31	8.27	38.02	2.91	3.73	28.39	–
	Eb (eV)	458.56	533.09	531.59	529.8	288.71	286.31	284.81	–
0.5 at% Zn^{2+}-doped TiO_2	at%	12.43	3.19	8.67	28.51	4.4	4.99	37.15	0.66
	Eb (eV)	458.56	533.45	531.83	529.88	288.74	286.32	284.82	1021.71

Table 2
Curve fitting result of high resolution XPS spectra for the O 1s region

Catalyst		O 1s (Ti–O)	O 1s (–OH)	O 1s (C–O)
Degussa P25	Eb (eV)	529.8	531.59	533.09
	r_i (%)	78.23	17.02	4.75
0.5 at% Zn^{2+}-doped TiO_2	Eb (eV)	529.88	531.83	533.45
	r_i (%)	70.62	21.48	7.90

3.5. PL spectrum of ZnO-doped TiO_2

Fig. 7 displayed the PL spectra of Degussa P25 and ZnO-doped TiO_2. A xenon UV–vis-near-IR excitation lamp was used to excite samples at 300 nm. Degussa P25 samples exhibited the highest PL emission peaks at 400–600 nm. The PL emission could be attributed to the surface state such as Ti^{4+}-OH, when excited with light having energies larger than the band gap of the samples [31]. For the 0.5 at% ZnO-doped TiO_2, the PL emission spectra were much lower than Degussa P25 and the peak of PL spectra shifted to shorter wavelength compared to Degussa P25. For the 10.0 at% ZnO-doped TiO_2, a green emission peak (573 nm) and a UV emission peak (380 nm) were observed in the PL spectra. As reported in the previous literature, the emission at 377 nm was corresponded to the band gap of ZnO material and assigned to the recombination of bound excitons of ZnO; the blue-green emission of ZnO was assigned to recombination of a photo-generated hole with a single ionized electron in the valence band [32–33]. Obviously, most of the surface of 10 at% ZnO–anatase–rutile was coated by ZnO particles. Since PL emission was the result of the recombination of excited electrons and holes, the lower PL intensity of the modified sample indicated a lower recombination rate of excited electrons and holes [34]. As shown in Fig. 7, the 0.5 at% ZnO-doped TiO_2 had the lowest recombination rate of electrons and holes among the three samples, leading to the highest photocatalytic oxidation activity.

3.6. The photocatalytic activity of ZnO-doped TiO_2

Experimental study to remove NO from a gaseous phase was carried out in the continuous-flow reactor using different catalysts. After a stabilized period for about 1 h, outlet NO concentration became the same as that of inlet gas and then the experiment started by turning on the UV lamp. In this experiment, the steady state was defined as the situation after 120 min reaction, since the variation of the outlet concentration of the NO was less than 5%.

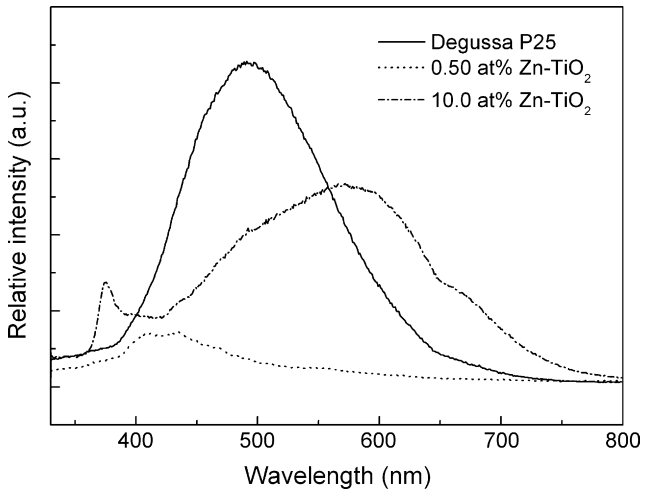

Fig. 7. The photoluminescence spectra of Degussa P25 and Zn^{2+}-doped TiO_2 particles.

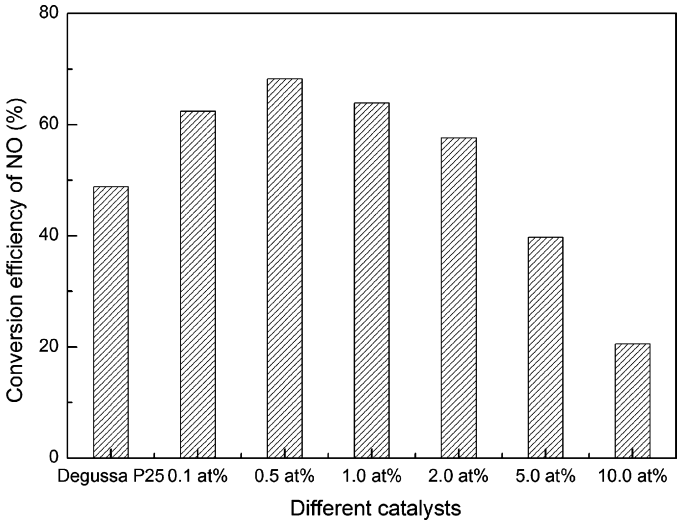

Fig. 8. NO conversion efficiency of catalysts with different zinc ions doping concentration (125 W Hg-arc lamp; relative humidity: 80%; O_2 concentration: 21%; space time: 10 s).

Fig. 8 showed the photocatalytic oxidation activity of nitric oxide over Degussa P25 and ZnO-doped TiO_2 with different doping concentration of zinc ions. With the zinc ions doping concentration of 0 (Degussa P25), 0.1, 0.5, 1.0, 2.0, 5.0 and 10.0 at%, the photocatalytic oxidation activities were 48.8, 62.4, 68.2, 63.9, 57.6, 39.7 and 20.5%. It indicated that the ZnO doping on the TiO_2 surface improved the photocatalytic oxidation activity of nitric oxide greatly. With 0.5 at% ZnO doping, the photocatalytic activity of the catalyst reached its highest value, which was nearly 20% higher than the pure Degussa P25. This result agreed well with the analysis results from XPS spectra and PL spectra. For the 0.5 at% ZnO-doped TiO_2, the hydroxyl content on the catalyst surface was improved and the recombination rate of electrons and holes was reduced compared with Degussa P25. Furthermore, from Fig. 8 it was also found that the ZnO doping concentration higher than 2.0 at% was not favorable for the photocatalytic oxidation activity of nitric oxide.

4. Discussion

It was reported that ZnO had the same band gap energy of anatase TiO_2 (3.2 eV) and similar electronic properties, but its valence band was higher than anatase [35]. After the doping of ZnO, ZnO dispersed on the TiO_2 surface might involve some charge transfer between anatase and rutile during UV-light illumination due to the difference in the energy band position. Thus, there existed a cooperative relationship between ZnO, anatase and rutile. A reaction mechanism of NO on ZnO-doped TiO_2 was proposed and shown in Fig. 9 [9,36,37]. From Fig. 9, the valence band of ZnO was higher than that of anatase, and the conduction band of anatase was higher than that of rutile. After the irradiation of UV-light, the electrons and holes were generated on the anatase surface. Then the generated holes could transfer from anatase to ZnO, while the generated electrons could move into rutile from anatase. Such a coupled effect among three semiconductors could decrease the recombination rate of electrons and holes. The improved hydroxyl content on photocatalyst surface interrupted the formation of adsorbed nitrolysis on the ZnO surface and formed hydroxyl radical under UV-light irradiation. Thus, the photocatalytic oxidation activity of ZnO-doped TiO_2 was then improved. Also, it was found that high doping concentration was

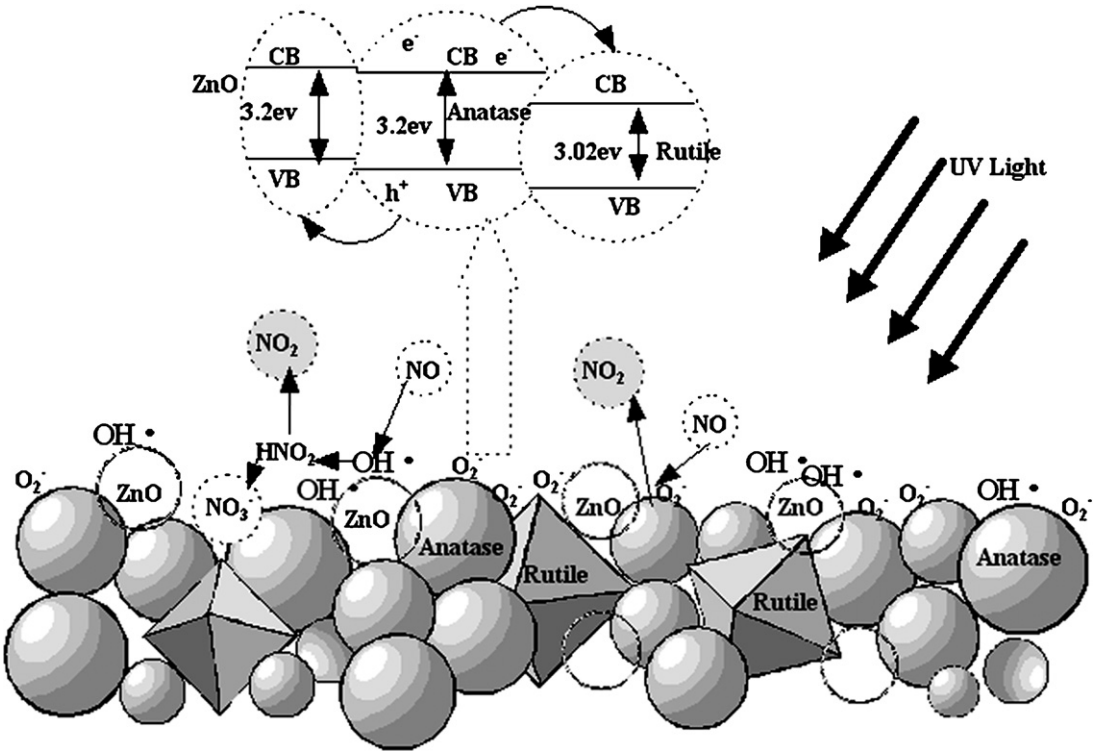

Fig. 9. Proposed photocatalytic reaction mechanism of NO on Zn^{2+}-doped TiO_2.

not beneficial to the photocatalytic activity because abundant ZnO particles on TiO_2 surface would become the new center of recombination.

5. Conclusion

The ZnO-doped TiO_2 gave an improved photocatalytic oxidation activity of NO compared with pure Degussa P25. Since the doping of ZnO particles could decrease the recombination rate of electrons and holes and improve the content of hydroxyl on the catalyst surface. Under the optimal doping concentration (0.5 at% Zn^{2+}), the photocatalytic activity of ZnO-doped TiO_2 was nearly 20% higher than the pure Degussa P25. However, high doping concentration was not beneficial to the photocatalytic activity because abundant ZnO particles on TiO_2 surface would become the new recombination center for electrons and holes.

Acknowledgement

This project was financially supported by the New Century Excellent Scholar Program of Ministry of Education of China (NCET-04-0549).

References

[1] T. Castro, S. Madronich, S. Rivale, A. Muhlia, B. Mar, Atmos. Environ. 35 (2001) 1765–1772.
[2] A. Farrell, Energy Policy 29 (2001) 1061–1072.
[3] M. Radojevic, Environ. Pollut. 102 (1998) 685–689.
[4] C.A. Jones, D. Stec, S.C. Larsen, J. Mol. Catal. A: Chem. 212 (2004) 329–336.
[5] R.M. Heck, Catal. Today 53 (1999) 519–523.
[6] H. Takeuchi, M. Ando, N. Kizawa, Ind. Eng. Chem. Proc. Des. Dev. 16 (1977) 303–308.
[7] L. Chen, J.-W. Lin, C.-L. Yang, Environ. Prog. 21 (2002) 225–230.
[8] S. Devahasdin, C. Fan Jr., K. Li, D.H. Chen, J. Photochem. Photobiol. A 156 (2003) 161–170.
[9] H.Q. Wang, Z.B. Wu, W.R. Zhao, B.H. Guan, Chemosphere 66 (2007) 185–190.
[10] T. Ibusuki, K. Takeuchi, J. Mol. Catal. 88 (1994) 93–102.
[11] C.H. Ao, S.C. Lee, C.L. Mak, L.Y. Chan, Appl. Catal. B: Environ. 42 (2003) 119–129.
[12] J.S. Dalton, P.A. Janes, N.G. Jones, J.A. Nicholson, K.R. Hallam, G.C. Allen, Environ. Pollut. 120 (2002) 415–422.
[13] H. Ichiura, T. Kitaoka, H. Tanaka, Chemosphere 51 (2003) 855–860.
[14] K. Hashimoto, K. Wasada, M. Osaki, E. Shono, K. Adachi, N. Toukai, H. Kominami, Y. Kera, Appl. Catal. B: Environ. 30 (2001) 429–436.
[15] F.B. Li, X.Z. Li, C.H. Ao, M.F. Hou, S.C. Lee, Appl. Catal. B: Environ. 54 (2004) 275–283.
[16] H.G. Yu, S.C. Lee, J.G. Yu, C.H. Ao, J. Mol. Catal. A: Chem. 246 (2006) 206–211.
[17] M.R. Hoffmann, S.T. Martin, W. Choi, D.W. Bahnemann, Chem. Rev. 95 (1995) 69–96.
[18] M.I. Litter, J.A. Navío, J. Photochem. Photobiol. A: Chem. 98 (1996) 171–181.
[19] J.A. Navío, J.J. Testa, P. Djedjeian, J.R. Padrón, D. Rodríguez, M.I. Litter, Appl. Catal. A: Gen. 178 (1999) 191–203.
[20] J.C.S. Wu, Y.T. Cheng, J. Catal. 237 (2006) 393–404.
[21] Y. Liu, H.Q. Wang, Z.B. Wu, J. Environ. Sci.-China 19 (2007) 1505–1509.
[22] D.W. Kim, S. Lee, H.S. Jung, J.Y. Kim, H. Shin, K.S. Hong, Int. J. Hydrogen Energy 32 (2007) 3137–3140.
[23] G. Marcì, V. Augugliaro, M.J. López-Muñoz, C. Martín, L. Palmisano, V. Rives, M. Schiavello, R.J.D. Tilley, A.M. Venezia, J. Phys. Chem. B 105 (2001) 1033–1040.
[24] G. Marcì, V. Augugliaro, M.J. López-Muñoz, C. Martín, L. Palmisano, V. Rives, M. Schiavello, R.J.D. Tilley, A.M. Venezia, J. Phys. Chem. B 105 (2001) 1026–1032.
[25] C. Wang, B.-Q. Xu, X.M. Wang, J.C. Zhao, J. Solid State Chem. 178 (2005) 3500–3506.
[26] J.-C. Xu, Y.-L. Shi, J.-E. Huang, B. Wang, H.-L. Li, J. Mol. Catal. A: Chem. 219 (2004) 351–355.
[27] J.G. Yu, X.J. Zhao, Q.N. Zhao, G. Wang, Mater. Chem. Phys. 68 (2001) 253–259.
[28] J.G. Yu, G.H. Wang, B. Cheng, M.H. Zhou, Appl. Catal. B: Environ. 69 (2006) 171–180.
[29] J.G. Yu, X.J. Zhao, Mater. Res. Bull. 36 (2001) 97–107.
[30] S.J. Liao, H. Donggen, D.H. Yu, Y.L. Su, G.Q. Yuan, J. Photochem. Photobiol. A: Chem. 168 (2004) 7–13.
[31] J.K. Zhou, M. Takeuchi, A.K. Ray, M. Anpo, X.S. Zhao, J. Colloid Interface Sci. 311 (2007) 497–501.
[32] X.Z. Wang, Q.P. Ding, H.B. Huang, S.G. Yang, Phys. Lett. A 365 (2007) 175–179.
[33] Y.L. Wu, A.I.Y. Tok, F.Y.C. Boey, X.T. Zeng, X.H. Zhang, Appl. Surf. Sci. 253 (2007) 5473–5479.
[34] J.C. Yu, W.K. Ho, J.G. Yu, S.K. Hark, K. Iu, Langmuir 19 (2003) 3889–3896.
[35] B. Pal, M. Sharon, Mater. Chem. Phys. 76 (2002) 82–87.
[36] Z.-H. Yuan, J.-H. Jia, L.-D. Zhang, Mater. Chem. Phys. 73 (2002) 323–326.
[37] L.Q. Jing, B.F. Xin, F.L. Yuan, L.P. Xue, B.Q. Wang, H.G. Fu, J. Phys. Chem. B 110 (2006) 17860–17865.